Results in Physics 54 (2023) 107107

Contents lists available at ScienceDirect

Results in Physics

journal homepage: www.elsevier.com/locate/rinp

A novel metal-mode-filtered vertical-cavity surface-emitting laser with 8 μm oxide aperture and single mode output

Jingfei Mu [a,b], Yinli Zhou [a,*], Xing Zhang [a], Jianwei Zhang [a], Chao Chen [a], Zhuo Zhang [a], Tianjiao Liu [a], Yuqi Xia [a,b], Yuehui Xu [a,b], Jingjing Sun [a,b], Haopeng Bai [a,b], Yongqiang Ning [a], Lijun Wang [a]

[a] State Key Laboratory of Luminescence and Applications, Changchun Institute of Optics, Fine Mechanics and Physics, Chinese Academy of Sciences, Changchun, Jilin 130033, China
[b] University of Chinese Academy of Sciences, Beijing 100049, China

ARTICLE INFO

Keywords
VCSEL
Metal-filter
Single mode
Electric-thermal simulation

ABSTRACT

In this study, a new theoretical calculation of metal-mode-filtered vertical-cavity surface-emitting laser (MMF-VCSEL) is proposed. The optimized number of P-DBR and the metal layer thickness are used. The effects of the metal mode filtered structure on the threshold gain of different transverse modes is analyzed. The MMF-VCSEL can operate in fundamental transverse mode under 8 μm oxide aperture compared with the conventional oxide-confined VCSEL. Benefit from the large oxide aperture and small metal aperture, the current crowding effect is effectively avoided and the heat distribution inside the VCSEL is improved.

Introduction

Vertical-cavity surface-emitting lasers (VCSELs) are a unique type of semiconductor laser. Due to its advantages of small size, low threshold current, single longitudinal mode, fast modulation speed, low power consumption and easy integration [1,2], VCSELs have become one of the most important semiconductor lasers in the market at present. In gas sensing [3,4], laser printing [5], chip atomic clock [6] and other applications [7,8], VCSEL is required to operate in single transverse mode. Single longitudinal mode is an inherent characteristic of VCSELs, but its large transverse size usually causes multiple transverse modes operation [9].

In conventional oxide-confined VCSELs, the oxide aperture diameter is restricted to around 3 μm by the single-mode condition [10]. Small oxide aperture will cause carrier accumulation and large thermal resistance, which will increase the temperature in the active region and eventually lead to power saturation of VCSEL. In order to make VCSEL work in single transverse mode under large oxide aperture (> 4 μm), various alternative approaches have been developed, including photonic crystal VCSELs [11–13], Surface relief VCSELs [14,15], Zn diffusion VCSELs [16], anti-resonant reflecting optical waveguide VCSELs [17], Surface grating VCSELs [18,19].

Most of the above methods increase the optical loss difference between fundamental mode and higher order modes by tailoring the top DBR of VCSEL, so as to realize the single mode operation under large oxide aperture. The spatial distribution and mode gain of each transverse mode do not change. In addition, because the metal aperture at the outlet of VCSEL is larger than the oxide aperture, carrier crowding effect still exists inside the device to affect the single-mode stability of VCSEL [20]. The majority of reported studies used metal hole to improve the side mode suppression ratio without considering the effect of the thickness of the metal layer [21,22].

In this paper, we present a new theoretical calculation of MMF-VCSEL. The structure of MMF-VCSEL differs from conventional oxide limited VCSELs in the optimized P-DBR number (8 pairs) and metal layer thickness (900 nm). By using a metal aperture smaller than the oxide aperture, the higher order modes in VCSEL is scattered more strongly than the fundamental mode, increasing the mode loss difference between the fundamental mode and the higher order modes. The 3 μm metal aperture and 8 μm oxide aperture effectively improves the current crowding effect, making the carrier distribution overlapped with the fundamental mode optical distribution better, further increasing the stability of the fundamental mode, and improving the heat distribution inside VCSEL.

* Corresponding author.
E-mail address: zhouyinli@ciomp.ac.cn (Y. Zhou).

https://doi.org/10.1016/j.rinp.2023.107107
Received 23 August 2023; Received in revised form 15 October 2023; Accepted 19 October 2023
Available online 20 October 2023

Device structure

The device structure diagram of MMF-VCSEL is shown in Fig. 1(a). N-DBR is composed of 34 pairs of $Al_{0.12}Ga_{0.88}As/Al_{0.9}Ga_{0.1}As$. P-DBR is composed of 8 pairs of $Al_{0.12}Ga_{0.88}As/Al_{0.9}Ga_{0.1}As$ and 7 pairs of SiO_2/Nb_2O_5. The active region consists of three pairs of $Al_{0.3}Ga_{0.7}As/GaAs$ as potential barriers and quantum Wells. The oxide layer is realized with a 30 nm thick $Al_{0.98}Ga_{0.02}As$ layer. A part of $Al_{0.98}Ga_{0.02}As$ is transformed into amorphous $(Al_xGa_{1-x})_2O_3$ to form oxide aperture after wet oxidation. A graphic metal layer is deposited on the surface of the $Al_{0.12}Ga_{0.88}As/Al_{0.9}Ga_{0.1}As$ layers of the P-DBR, which is used as a metal-filter layer and P electrode. The upper surface of the P-type electrode is patterned SiO_2/Nb_2O_5 dielectric film layers. Fig. 1(b) illustrates the relationship between material gain and reflectivity of MMF-VCSEL with respect to wavelength. The optimal alignment of both parameters is attained at the central wavelength of 850 nm.

Simulation analysis and conclusions

In order to increase the mode volume of the fundamental mode light to increase output power and reliability, an oxide aperture size of 8 μm was used in MMF-VCSEL. Using Maxwell's equations and the boundary conditions at the core-cladding interface one can find the transverse electromagnetic modes supported by the waveguide, which are characterized by their propagation constants and characteristics field distributions in the transverse plane [23]. The optical field distribution of the conventional single mode VCSEL(SM-VCSEL) and MMF-VCEL with 8 μm oxide aperture are shown in Fig. 2, simulated by COMSOL (V 4.1). As depicted in Fig. 2(a), the P-DBR of traditional SM-VCSEL is composed of 22 pairs of $Al_{0.12}Ga_{0.88}As/Al_{0.9}Ga_{0.1}As$, the first three transverse modes LP_{01}, LP_{11} and LP_{21} are all well confined within the oxide aperture with little scattering. This indicates that in traditional SM-VCSEL, the higher-order mode and the fundamental mode are subject to almost the same mode gain and mirror loss, and therefore prone to multi-mode operation. In the MMF-VCSEL, a 3 μm metal aperture is adopted, as shown in Fig. 2(b), the metal aperture causes the high-order mode to suffer strong scattering, which leads to decreased mode gain and increased optical loss of the high-order mode, so that the MMF-VCSEL can keep the single-mode operation.

The lasing threshold condition of VCSEL can be expressed as:

$$\Gamma g_{th} = \alpha_{in} + \alpha_{mirr} \tag{1}$$

Where Γ is the optical confinement factor, Γ represents the limiting effect of waveguide structures on both sides of the active region on the light field. A higher Γ results in increased field intensity within the active region, leading to a higher probability of electron-hole recombination in that area. And the device threshold can be effectively reduced. Γ is expressed as:

$$\Gamma = \frac{\int |E|^2_{active}}{\int |E|^2_{device}} \tag{2}$$

g_{th} is the threshold material gain, and Γg_{th} is called threshold gain. The α_{in} is the intrinsic loss, and α_{mirr} is the mirror loss expressed by equation (3). It represents the light leakage loss caused by the light reflected by the DBR on both sides.

$$\alpha_{mirr} = \frac{1}{L_{eff}} ln \frac{1}{\sqrt{R_t R_b}} \tag{3}$$

Where L_{eff} is the effective cavity length of the VCSEL, R_t and R_b denote the reflectivity of the top mirror and the bottom DBR. The reflectivity of the metal layer thickness ranging from 0 to 3 μm is shown in Fig. 3 (a). The reflectivity changes periodically with an increase of the metal thickness. The metal layer is between the periodic DBR and the dielectric film, and this periodic change is determined by the Bragg reflection condition. Within a specific thickness range, where the phase satisfies the condition, the reflectivity will stay at a high level due to constructive interference. However, when interference cancellation occurs, the reflectivity will decrease. The light absorption of the metal layer is fitted to the reflectivity formula. It can be expressed as:

$$R' = R^*(1 - \Gamma_{metal}*(1 - e^{-\alpha^* z})) \tag{4}$$

Where R is the reflectivity without considering the absorption of the metal layer, Γ_{metal} is the light limiting factor of the metal layer, α is the absorption coefficient of the metal and z is the thickness of the metal layer. The mode loss of different modes can be obtained by calculating the reflectance of regions with and without metal layers respectively, and then weighting them according to the proportion of light distribution in different regions. The correlation between the metal layer thickness and α_{mirr} of the MMF-VCSEL is presented in Fig. 3 (b). The α_{mirr} of LP_{01} and LP_{11} modes are both increase with the metal thickness rises. And the difference between LP_{01} and LP_{11} increases with the thickness of the metal layer. High fundamental mode loss is not desirable, so a metal layer thickness of 900 nm was eventually determined. The results in [24] can be used as a reference for modes damage. The difference in values may be due to differences in calculation methods and device structures. The mode damage difference of MMF-VCSEL can bring higher single-mode operating current compared with the conventional SM-VCSEL. It benefits to the higher single-mode output power.

Fig. 4 (a) shows the optical confinement factor difference between LP_{01} and LP_{11} modes of the MMF-VCSEL and traditional SM-VCSEL at different metal and oxide aperture diameters. For MMF-VCSEL, the oxide aperture diameter is fixed to 8 μm and the diameter of the metal aperture change from 2 μm to 8 μm. Compared with traditional SM-VCSEL, MMF-VCSEL shows a greater difference in light confinement factor, which is due to the strong scattering effect of metal aperture on the light mode in VCSEL. This scattering effect decreases with the increase of the metal aperture size. When the metal aperture size is the

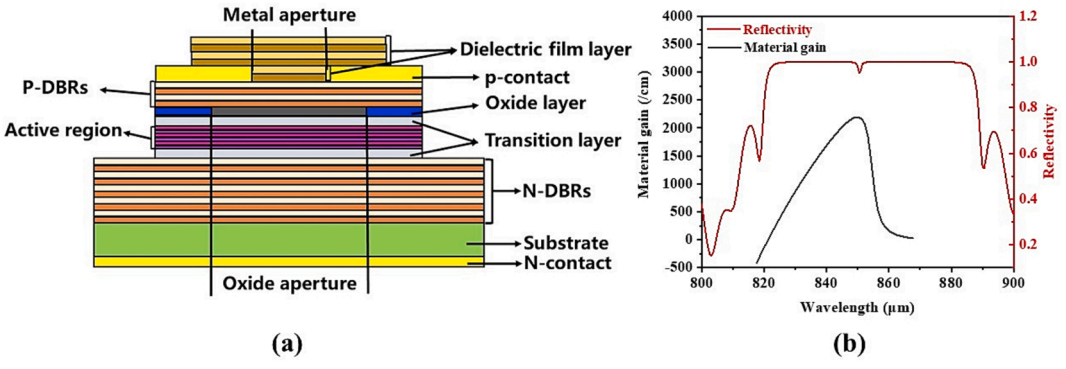

Fig. 1. (a) Structure diagram of MMF-VCSEL. (b) Material gain and reflectivity vary along wavelength.

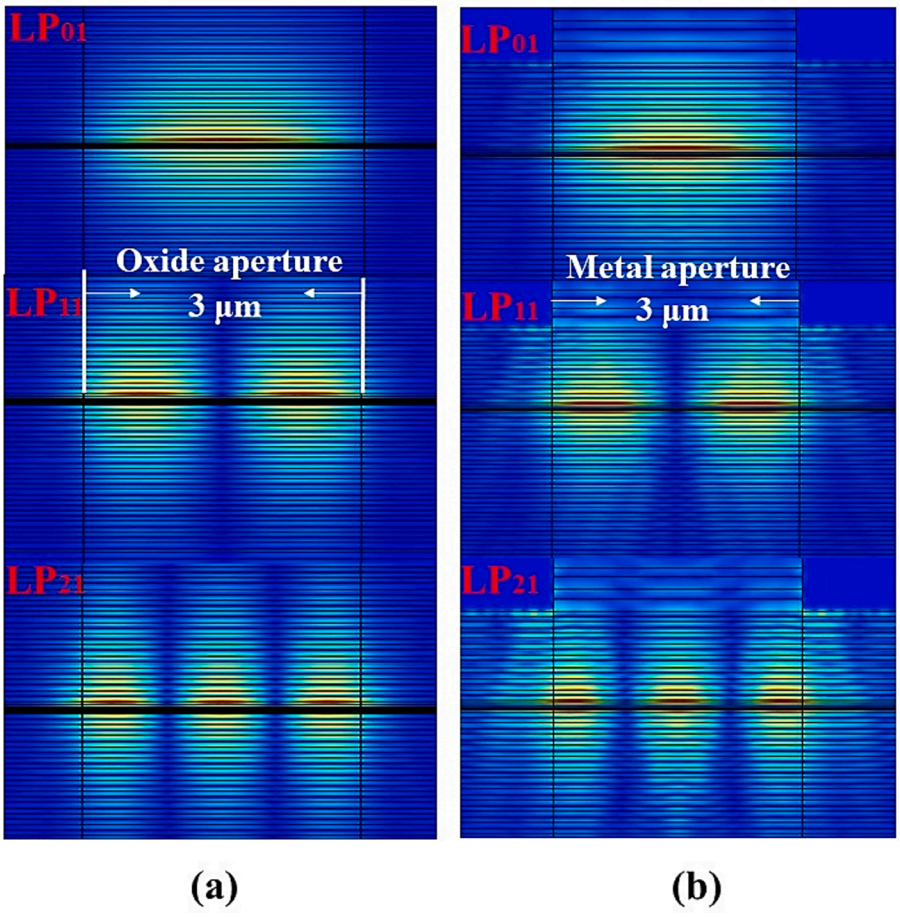

Fig. 2. Optical field distribution inside cavities of (a) the conventional SM-VCSEL and (b) MMF-VCSEL.

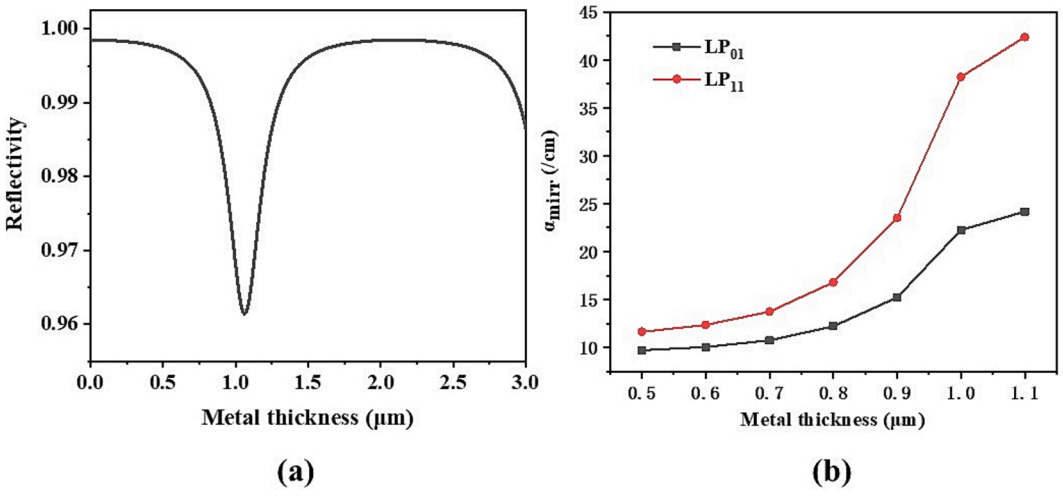

Fig. 3. (a) Reflectivity of the top mirror varies with the metal thickness. (b) Modes LP_{01} and LP_{11} losses of MMF-VCSEL vary along the metal thickness with 3 μm metal aperture.

same as the oxide aperture size, the metal aperture loses its modulating effect on the transverse mode of VCSEL. The mode loss difference between the LP_{01} and LP_{11} modes for both the MMF-VCSEL and conventional SM-VCSEL as a function of aperture size is shown in Fig. 4(b). Because the higher order modes are more distributed in the metal layer with low reflectance, MMF-VCSEL has a larger loss difference between the fundamental mode and the higher order mode. Due to the weakening of the scattering effect of the metal aperture, the mode loss difference also decreases with the increase of the metal aperture diameter. The above results show that compared with traditional SM-VCSEL, MMF-VCSEL has stronger scattering effect on transverse optical mode, and makes the fundamental mode have larger optical mode gain and lower optical loss than the high order modes. Therefore, MMF-VCSEL can realize more stable fundamental mode operation.

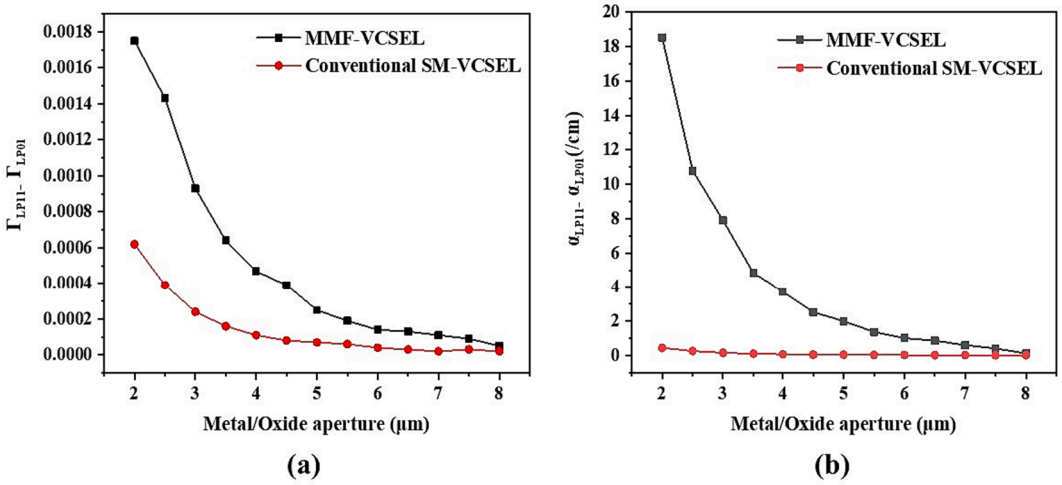

Fig. 4. (a) Optical confinement factor difference and (b) Difference of mode losses of LP_{01} and LP_{11} between MMF-VCSEL and conventional SM-VCSEL along metal/oxide aperture.

Due to the combination of a larger metal contact ring with a smaller oxide aperture, there is a current crowding effect exists in traditional SM-VCSEL [25], which shows a stronger injection close to the oxide aperture rim than in the center. This uneven current distribution will lead to the spatial hole burning effect and ultimately affect the mode stability of VCSEL [26]. The current crowding effect is greatly improved in the novel MMF-VCSEL design, which benefits from the smaller metal contact ring and larger oxide aperture, since the current tends always to follow the shortest path between the two electrodes [25]. When the metal aperture is larger than oxide aperture, the shortest path passes through the edge of the oxidation hole, resulting in the current crowding effect. At the large oxide aperture and small metal aperture, the shortest path is closer to the oxidation hole center, and the current crowding effect is also improved. The active region heat model based on carrier injection heat production mechanism was established based on finite element method [27–29]. SM-VCSEL and MMF-VCSEL device model are established by COMSOL (V 4.1), and the active region temperature variation and current density distribution were simulated.

Fig. 5 displays one-dimensional distribution of normalized current density in the active regions of the MMF-VCSEL and conventional VCSELs with 3 μm and 8 μm oxide aperture. The conventional VCSELs has 10 μm metal aperture, and the MMF-VCSEL has 8 μm oxide aperture and 3 μm metal aperture. Due to the carrier crowding effect, the traditional VCSELs present a cat's ear shaped current distribution along the transverse direction. At the same oxide aperture of 8 μm, MMF-VCSEL has a more uniform current density distribution than traditional oxide limited VCSEL. It shows that the presence of metal layer does have a positive effect on the current density distribution of MMF-VCSEL.

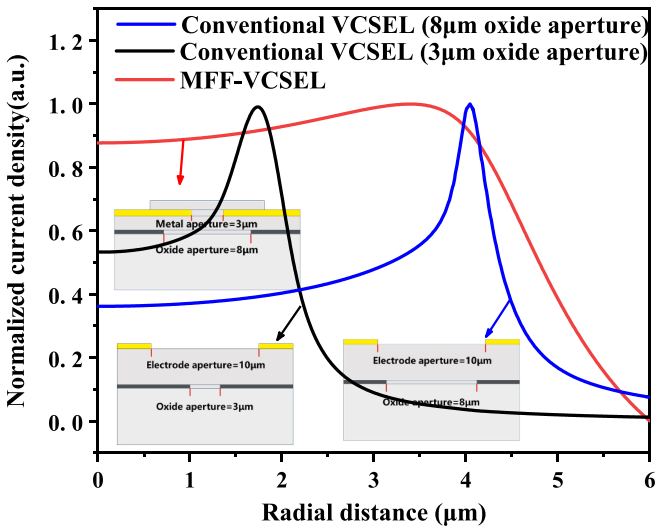

Fig. 5. Normalized current density distribution in the active regions of the MMF-VCSEL and conventional SM-VCSEL with 3 μm and 8 μm oxide aperture.

Due to the high resistance and thermal resistance caused by small oxide aperture, conventional SM-VCSEL is prone to thermal rollover, and the operating current of is generally below 5 mA [30]. Benefits from the large oxide aperture and small metal aperture, MMF-VCSEL is promising for single-mode operation at larger current with lower device temperature. Fig. 6 depicts the one-dimensional distribution of active region temperature for MMF-VCSEL and conventional SM-VCSEL at varying injection currents. Even at higher operating currents, the MMF-VCSEL still has lower device temperatures than the traditional SM-VCSEL. Although large oxide aperture can lead to an increase in device threshold current, the greater thermoelectric performance makes it possible for MMF-VCSEL to achieve stable single-mode output with high power.

Conclusion

In this study, a novel MMF-VCSEL design that can achieve single-mode output at a large oxide aperture is presented. The simulation results show that MMF-VCSEL realizes the transverse mode control in VCSEL through the strong light scattering effect of metal aperture, which is different from the mode control method achieved by oxide aperture in the existing reports. Benefit from the 8 μm oxide aperture and 3 μm metal aperture of MMF-VCSEL, the current crowding effect is improved, and the device has better electro-thermal performance. It is possible for MMF-VCSEL to maintain stable high-power single-mode operation at higher current.

CRediT authorship contribution statement

Jingfei Mu: Conceptualization, Data curation, Formal analysis, Investigation, Methodology, Software, Validation, Visualization, Writing – original draft, Writing – review & editing. **Yinli Zhou:** Conceptualization, Formal analysis, Funding acquisition, Methodology, Project administration, Resources, Software, Supervision, Validation. **Xing Zhang:** Project administration, Resources. **Jianwei Zhang:** Funding acquisition, Project administration. **Chao Chen:** Resources. **Zhuo Zhang:** Formal analysis. **Tianjiao Liu:** Data curation,

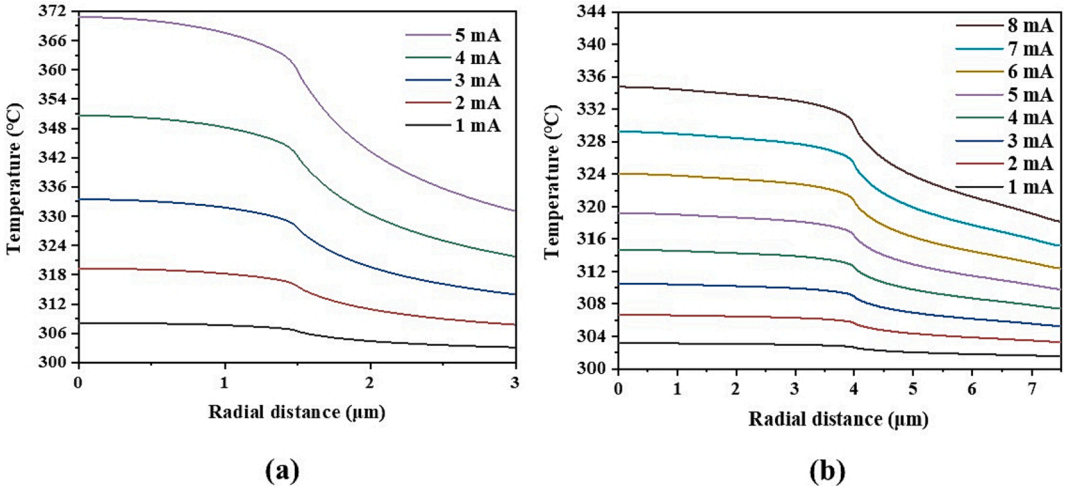

Fig. 6. Temperature distribution of the active region along injection current for (a) traditional SM-VCSEL and (b) MMF-VCSEL.

Investigation. **Yuqi Xia:** Formal analysis, Investigation. **Yuehui Xu:** Data curation. **Jingjing Sun:** Investigation. **Haopeng Bai:** Investigation. **Yongqiang Ning:** Resources. **Lijun Wang:** Resources.

Declaration of Competing Interest

The authors declare that they have no known competing financial interests or personal relationships that could have appeared to influence the work reported in this paper.

Data availability

Data will be made available on request.

References

[1] Larsson A. Advances in VCSELs for communication and sensing. IEEE J Selected Top Quantum Electron 2011;17(6):1552–67. https://doi.org/10.1109/JSTQE.2011.2119469.
[2] Kasukawa A. VCSEL technology for green optical interconnects. J IEEE Photon J 2012;4(2):642–6. https://doi.org/10.1109/JPHOT.2012.2190723.
[3] Lan L, Chen J, Zhao X, Ghasemifard H. VCSEL-based atmospheric trace gas sensor using first harmonic detection. IEEE Sensors J 2019;19(13):4923–31.
[4] Witzel O, Klein A, Meffert C, Wagner S, Kaiser S, Schulz C, et al. VCSEL-based, high-speed, in situ TDLAS for in-cylinder water vapor measurements in IC engines. J Optics Express 2013;21(17):19951.
[5] Nakamura T, Nakayama H, Omori S, et al. Single-Mode Oxide-Confined VCSEL for Printers and Sensors; proceedings of the 2006 1st Electronic Systemintegration Technology Conference, F 5-7 Sept. 2006, 2006. https://doi.org/10.1109/ESTC.2006.279982.
[6] Kroemer E, Rutkowski J, Maurice V, et al. Characterization of commercially available vertical-cavity surface-emitting lasers tuned on Cs D1 line at 894.6 nm for miniature atomic clocks. J Appl Opt 2016;55(31):8839–47. https://doi.org/10.1364/AO.55.008839.
[7] Simpanen E, Gustavsson JS, Larsson A, Karlsson M, Sorin WV, Mathai S, et al. 1060 nm single-mode VCSEL and single-mode fiber links for long-reach optical interconnects. J Lightwave Technol 2019;37(13):2963–9.
[8] Li M-J, Li K, Chen X, Mishra SK, Juarez AA, Hurley JE, et al. Single-mode VCSEL transmission for short reach communications. J Lightwave Technol 2021;39(4):868–80.
[9] Jung C, Jäger R, Grabherr M, et al. 4.8 mW singlemode oxide confined top-surface emitting vertical-cavity laser diodes [J/OL] 1997, 33(21):1790-1. [https://digital-library.theiet.org/content/journals/10.1049/el_19971207.
[10] Grabherr M, Jager R, Michalzik R, Weigl B, Reiner G, Ebeling KJ. Efficient single-mode oxide-confined GaAs VCSEL's emitting in the 850-nm wavelength regime. J IEEE Photon Technol Lett 1997;9(10):1304–6.
[11] Alias MS, Shaari S, Leisher PO, Choquette KD. Single transverse mode control of VCSEL by photonic crystal and trench patterning. J Photon Nanostruct-Fundam Appl 2010;8(1):38–46.
[12] Liu Q, Bin J, Feng K, Cheng L, Zhao L, Wu G, et al. Design of GaN-based photonic crystal surface emitting lasers with top TiO2 photonic crystals. J Results Phys 2022;33:105164.
[13] Czyszanowski T, Dems M, Panajotov K. Single mode condition and modes discrimination in photonic-crystal 1.3 μm AlInGaAs/InP VCSEL. J Optics Express 2007;15(9):5604–9. https://doi.org/10.1364/OE.15.005604.
[14] Wang X, Hao YQ, Yan CL, et al. High power single-higher-mode VCSEL with inverted surface relief, J Infrared Millimeter Waves, 2018, 37(2): 168-72. https://doi.org/10.11972/j.issn.1001-9014.2018.02.007.
[15] Haglund A, Gustavsson JS, Vukusic J, Modh P, Larsson A. Single fundamental-mode output power exceeding 6 mW from VCSELs with a shallow surface relief. J IEEE Photon Technol Lett 2004;16(2):368–70.
[16] Khan Z, Shih JC, Cheng CL, et al. High-power and highly single-mode Zn-diffusion VCSELs at 940 nm wavelength; proceedings of the 2019 IEEE Photonics Conference (IPC), F 29 Sept.-3 Oct. 2019, 2019. https://doi.org/10.1109/IPCon.2019.8908460.
[17] Ledentsov NN, Shchukin VA, Kalosha VP, Ledentsov NN, Kropp J-R, Agustin M, et al. Anti-waveguiding vertical-cavity surface-emitting laser at 850 nm: From concept to advances in high-speed data transmission. J Optics Express 2018;26(1):445.
[18] Haglund E, Jahed M, Gustavsson JS, Larsson A, Goyvaerts J, Baets R, et al. High-power single transverse and polarization mode VCSEL for silicon photonics integration. J Optics Express 2019;27(13):18892.
[19] Li K, Chase C, Qiao PF, et al. Widely tunable 1060-nm VCSEL with high-contrast grating mirror. J Optics Express 2017;25(10):11844–54. https://doi.org/10.1364/oe.25.011844.
[20] Debernardi P. HOT-VELM: a comprehensive and efficient code for fully vectorial and 3-D hot-cavity VCSEL simulation. J IEEE J Quantum Electr 2009;45(8):979–92. https://doi.org/10.1109/JQE.2009.2016762.
[21] Ueki N, Sakamoto A, Nakamura T, Nakayama H, Sakurai J, Otoma H, et al. Single-transverse-mode 3.4-mW emission of oxide-confined 780-nm VCSELs. J IEEE Photon Technol Lett 1999;11(12):1539–41.
[22] Morgan RA, Guth GD, Focht MW, Asom MT, Kojima K, Rogers LE, et al. Transverse mode control of vertical-cavity top-surface-emitting lasers. J IEEE Photon Technol Lett 1993;5(4):374–7.
[23] Saleh BE, Teich MC. Fundamentals of photonics. John Wiley & sons; 2019.
[24] Ii X, Zhou Y, Zhang X, et al. High-power single-mode 894 nm VCSELs operating at high temperature (> 2 mW @ 365 K). J Appl Phys B 2022;128(1):16. https://doi.org/10.1007/s00340-021-07748-w.
[25] Debernardi P. Three-dimensional modeling of VCSELs, Michalzik R. VCSELs: fundamentals, technology and applications of vertical-cavity surface-emitting lasers. Berlin, Heidelberg; Springer Berlin Heidelberg. 2013: 77-117.
[26] Khan Z, Ledentsov N, Chorchos L, Shih J-C, Chang Y-H, Ledentsov NN, et al. Single-mode 940 nm VCSELs with narrow divergence angles and high-power performances for fiber and free-space optical communications. J IEEE Access 2020;8:72095–101.
[27] James F, Li Z, Weijian Y, et al. Heterogeneously-integrated VCSEL using high-contrast grating on silicon; proceedings of the ProcSPIE, F, 2015. https://doi.org/10.1117/12.2079732.
[28] Wang J, Savidis I, Friedman EG. Thermal analysis of oxide-confined VCSEL arrays. J Microelectr J 2011;42(5):820–5. https://doi.org/10.1016/j.mejo.2010.11.005.
[29] Jeong H, Choquette K D. Thermal modeling of transferred VCSELs; proceedings of the 2013 IEEE Photonics Conference, F 8-12 Sept. 2013, 2013. https://doi.org/10.1109/IPCon.2013.6656529.
[30] Ii X, Zhou Y, Zhang X, et al. High-power single-mode 894 nm VCSELs operating at high temperature (> 2 mW @ 365 K). J Appl Phys B 2022;128(1). https://doi.org/10.1007/s00340-021-07748-w.